Applied Physics B (2019) 125:73
https://doi.org/10.1007/s00340-019-7167-2

Applied Physics B
Lasers and Optics

Optical nonlinear absorption of a few-layer MoS_2 under green femtosecond excitation

Dmitry V. Khudyakov[1] · Andrey A. Borodkin[1] · Anatoly S. Lobach[2] · Danila D. Mazin[1] · Sergey K. Vartapetov[1]

Received: 29 September 2018 / Accepted: 5 March 2019 / Published online: 8 April 2019

Abstract
The nonlinear optical absorption of aqueous suspension with a few-layer (4–5 layers) molybdenum disulfide (MoS_2) was investigated by Z- and P-scan methods using second harmonic generation from Yb-doped femtosecond pulsed laser. Two regions with different nature of the nonlinear absorption were registered when the intensity of the incident radiation increased from low to high values. The 3-level model for one-photon transitions in the few-layer MoS_2 was proposed for describing the experimental data. Absorption cross sections and relaxation times for interband and intraband transitions under femtosecond excitation on 514 nm have been estimated.

1 Introduction

Layered MoS_2 as a two-dimensional semiconductor is a promising compound for use in film optoelectronics. In contrast to other two-dimensional material, graphene, MoS_2 has a band gap for photon energy in the visible spectral range, which can be used to create optoelectronic devices such as light-emitting diodes, solar cells and highly sensitive detectors of visible radiation [1]. Single-layer and few-layer MoS_2 as the most studied compounds among transition-metal dichalcogenides show a significant nonlinear optical response [2–5]. Using saturable absorbers based on films with MoS_2, the authors obtained Q-switching [6] and mode-locking [7] for pulsed lasing. The methods of mechanical and chemical exfoliation of crystalline MoS_2 to produce single-layered and few-layer flakes of submicron size, including different geometries, allow changing the nonlinear response over a wide range [8]. Despite the large number of experimental papers on this topic, the relaxation dynamics of photoexcited charge carriers and the mechanism of nonlinear optical absorption in single-layer and few-layer MoS_2 require further study, which gives the necessary information for designing the devices based on MoS_2.

2 Experimental methods and discussion

A water-soluble carboxymethylcellulose polymer (sodium salt of CMC of medium viscosity, Sigma) was used to prepare a stable suspension of few-layer sheets of MoS_2 in water. The suspension was prepared by dispersing 2H polytype of MoS_2 powder in an aqueous solution of 1 wt% CMC in a ultrasonic bath (Bandelin sonorex, 80 W, frequency 35 kHz) for 1 h at room temperature and then treated with an ultrasonic probe disperser (frequency 35 kHz, power 500W) inside the thermostat steel cup at a temperature of 24 °C for 8 h. Thereafter, the suspension was centrifuged at 5000 g for 30 min (Eppendorf centrifuge 5804) to remove large aggregates of MoS_2 particles. The top (~80%) of the homogeneous suspension above the precipitate was decanted, diluted 1:5 with an aqueous solution of 1 wt% CMC and this suspension was used for experiments. The absorption spectrum of the suspension is shown in Fig. 1. The optical spectrum has four absorption bands with maxima at 666, 608, ~440, and 395 nm, which corresponds to the A, B, C, and D absorption lines of MoS_2. The concentration of MoS_2 in the suspension was 0.027 mg/ml. Raman scattering spectra of the MoS_2 film on glass (a dried drop of a MoS_2 suspension in an aqueous solution of 1 wt% CMC) is shown in Fig. 2. Two bands corresponding to Raman modes E^1_{2g} and A_{1g} with frequency peaks at 383.1 and 407.4 cm^{-1} are observed in the spectrum,

✉ Dmitry V. Khudyakov
khudyakov@pic.troitsk.ru

[1] Prokhorov General Physics Institute of the Russian Academy of Sciences, Moscow, Russian Federation

[2] The Institute of Problems of Chemical Physics RAS, Academician Semenov av. 1, Chernogolovka, Moscow Region, Russian Federation

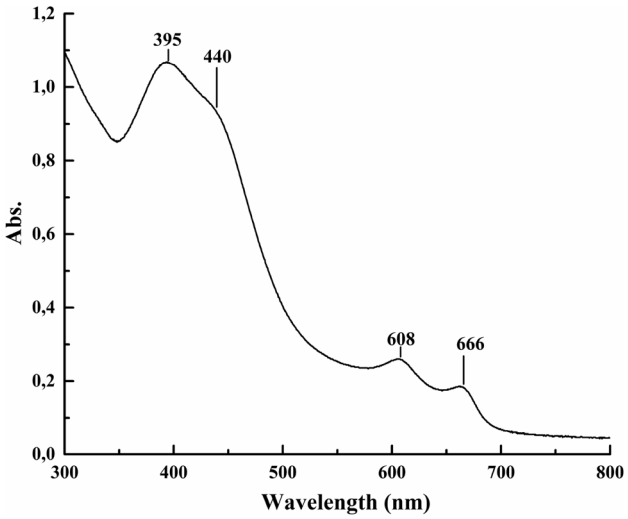

Fig. 1 Optical absorption spectrum of the aqueous suspension with MoS_2 (0.027 mg/ml MoS_2 in an aqueous solution 1% by weight CMC, 2 mm cell)

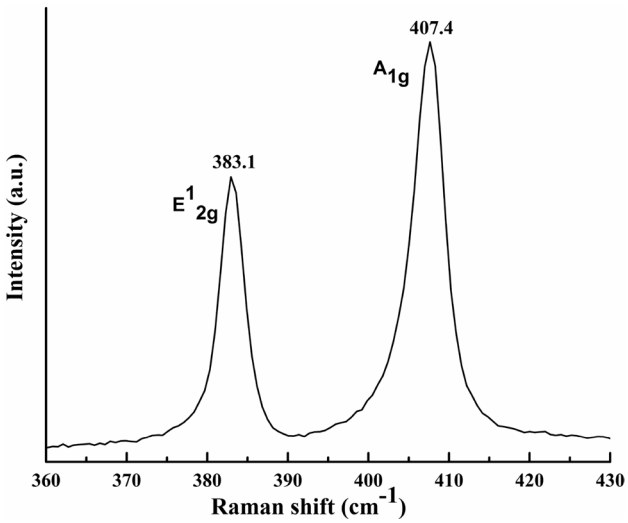

Fig. 2 Raman spectrum of the few-layer MoS_2 on a glass (a dried drop of a MoS_2 suspension in an aqueous solution of 1 wt% CMC). The spectrometer Horiba T64000 with excitation at 514 nm and the laser radiation power on the sample was 0.1 mW

respectively. The frequency difference is 24.3 cm^{-1}, which corresponds to 4–5 layers MoS_2 nanoflakes (for the original MoS_2 powder this difference is equal to 25.7 cm^{-1}) [9, 10].

Experimental P- and Z-scan techniques were used to measure the optical nonlinear characteristics of the aqueous suspension of MoS_2. In both methods, a pulsed Yb^{3+}KGW laser with a fundamental wavelength of 1028 nm and nonlinear crystal KDP for second harmonic generation at 514 nm with a pulse duration of 400 fs were used in experimental setup as it was described earlier in [11]. The repetition rate f of the pulses was 1 kHz, the energy in each pulse was $2 \div 10$ μJ at the second harmonic. Z-scan was carried out with open aperture scheme for recording only nonlinear absorption. The sample was a 2-mm-thick cell with an aqueous suspension of MoS_2 which was able to move along the laser beam (z-coordinate) near the focusing region. The radius of the beam r changed along optical axis achieving minimum of 55 μm in the focusing point ($z = 0$). The average power W that passed through the sample was recorded with a power meter and the peak intensity of the incident radiation was calculated from the expression:

$$I_0 \approx \frac{W}{\pi r^2 \times \tau_p \times f}, \quad (1)$$

where τ_p is the duration of the laser pulse (full width at half maximum of the profile). The incident peak intensity in Z-scan experiment depends on z-coordinate, the intensity monotonically decreases from zero point where it has maximal value. In the case of power scanning (P-scan), the sample was positioned exactly in the waist of the laser beam. The pump intensity was smoothly varied by rotating a half-wave plate mounted in front of the Glan–Thomson prism. In the experiments the optical transmittance—ratio of transmitted through the sample power-to-the incident power radiation—was measured. The solid curves for Z-scan on Fig. 3 and the grey curve for P-scan in Fig. 4 show how the experimental transmittance changes depending on incident peak intensity. The both experimental techniques showed the same behavior of the optical transmittance depending on the incident peak intensity.

By increasing the incident intensity up to 15 GW/cm^2 the nonlinear absorption of the sample was observed. If increased intensity was higher than 15 GW/cm^2, the

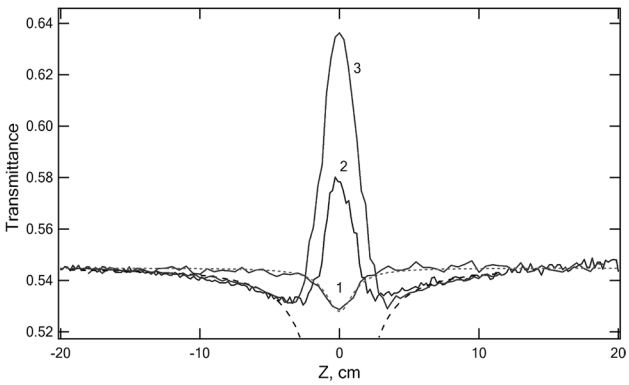

Fig. 3 Experimental Z-scan curves (solid lines) of the sample with few-layer MoS_2 measured at pulse energy of 0.3 μJ (curve 1), 1 μJ (curve 2) and 2 μJ (curve 3) on wavelength 514 nm. Dots line is the best approximation of the curve 1 using Eq. 9. Dotted line is the best approximation of wings for the curve 3 using Eq. 9

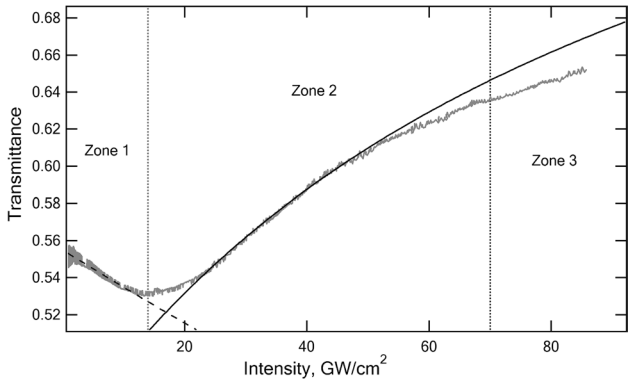

Fig. 4 Experimental P-scan curve (gray line) of the sample with few-layer MoS_2 on wavelength 514 nm and the best approximations in Zone 1 (dotted line) using Eq. 8, in Zone 2(solid line) using Eq. 12. Dots lines separate the intensity scale on three zones. *Zone 1* RSA on low intensity, *Zone 2* SA on high intensity, *Zone 3* area of the sample destruction

saturable absorption (SA) was registered up to the values of 70–80 GW/cm^2 at which the sample was damaged or boiled.

For theoretical evaluation of the experimental dependences we used 3-level scheme shown in Fig. 5a. The reason of such scheme for energy levels follows from calculations of the exciton states for 2H-MoS_2 performed in [12–14]. The Fig. 5b shows the calculated in [14] band structures of MoS_2 quadrilayer between K and Γ points in the Brillouin zone. The vertical arrows display the area of possible transitions with photon of our excitation light − 2.4 eV from the valence band state VB to the lower conduction band state CB1 and the next transitions to the upper conduction band state CB2.

After excitation with a pulse of intensity$I$(t) the changes of the carrier concentrations N_1, N_2, N_3 at the levels of the valence band (VB), the first conduction band (CB1) and the second conduction band (CB2), correspondingly, were described by the system of differential equations:

$$\frac{dN_1}{dt} = -\frac{\sigma_0 N_1}{\hbar\omega} I + \frac{N_2}{\tau_1} - \frac{\beta}{2\hbar\omega} I^2, \tag{2}$$

$$\frac{dN_2}{dt} = \frac{\sigma_0 N_1}{\hbar\omega} I - \frac{\sigma_1 N_2}{\hbar\omega} I - \frac{N_2}{\tau_1} + \frac{N_3}{\tau_2}, \tag{3}$$

$$\frac{dN_3}{dt} = \frac{\sigma_1 N_2}{\hbar\omega} I - \frac{N_3}{\tau_2} + \frac{\beta}{2\hbar\omega} I^2, \tag{4}$$

where σ_0 and σ_1 are the absorption cross sections for transitions VB→CB1 and CB1→CB2, respectively. β is the two-photon absorption coefficient, $\omega = 2\pi\nu$ is the angular frequency of the excitation light; τ_1, τ_2 are the interband and intraband relaxation time, respectively. The initial conditions for the solution of the system Eqs. (2–4) were chosen $N_2 = N_3 = 0$, $N_1 = N_0$ and N_0 is the photoinduced electron–hole density.

Absorption of the light as a function of a sample thickness is described by

$$\frac{dI}{dz} = -\sigma_0 N_1 I - \sigma_1 N_2 I - \beta I^2. \tag{5}$$

To determine interband relaxation time we used pump-to-probe experiment with picosecond time resolution. In this method, the sample was placed near the beam waist to achieve the necessary intensity of the pump pulse on wavelength of 514 nm. The peak intensity of the pump pulse in

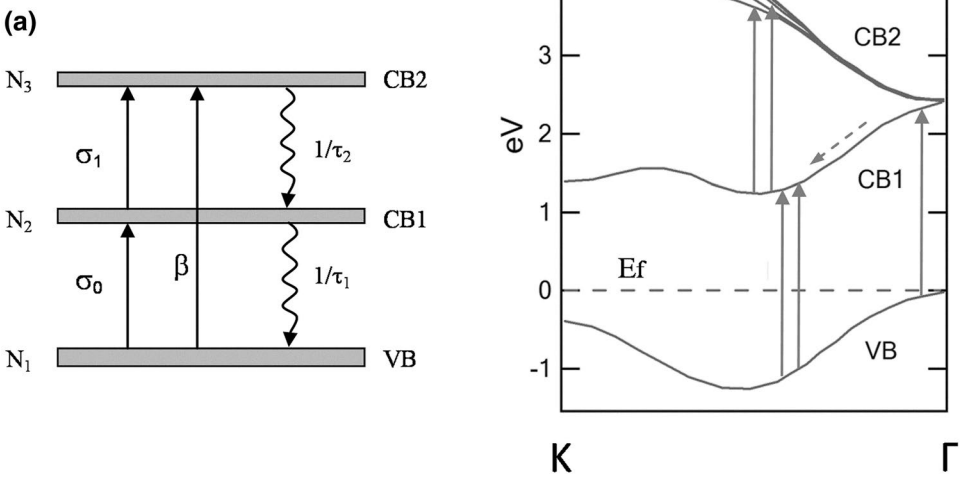

Fig. 5 **a** Energy-level scheme which was used for theoretical evaluation of the experimental data. **b** Band structures of MoS_2 quadrilayer adapted from [14], E_f—Fermi level. Vertical arrows indicate the possible transitions between states with energy distance corresponds to green photon − 2.4 eV. Dotted arrow—ultrafast carrier thermalization at lower-condition band state

the experiment was 17 GW/cm^2, where a predominantly nonlinear absorption is observed. The attenuated probe pulse on the same wavelength passed through the excitation region with a time delay and the average power of the probing radiation was recorded. The delay of the probe pulse with respect to the pump pulse was set by delay line. Time-resolved transmittance of the probe pulse in the picosecond time scale is presented on Fig. 6.

The time-dependent transmittance for the probe pulse is determined by the time dependence of the concentrations N_1 and N_2 in the system of Eqs. (2–4). As far as intraband relaxation time τ_2 lies in femtosecond time scale and condition $\tau_1 >> \tau_2$ is fulfilled, the kinetics of the transmittance in picosecond time range is determined mainly by relaxation time τ_1 and the system of only two first equations with term N_2/τ_1 in the right side. Solving Eqs. (2,3) together with Eq. 5 the time dependence of the transmittance described by

$$T(t) = T_0 \exp\left\{-\exp\left(-t/\tau_1\right)\left(\sigma_1 - \sigma_0\right)N_2(0)L\right\}, \quad (6)$$

where $T_0 = \exp(-\sigma_0 N_0 L)$, $N_2(0)$ is a concentration of the photoinduced carriers on lower-condition band state CB1 just after pulsed excitation and L is a sample length. Using Eq. 6 for approximation experimental curve on Fig. 6 one can obtain the interband relaxation time of the photoexcited carriers $\tau_1 = 20 \pm 2$ ps. The measured value of τ_1 is less than 70 ps obtained from the measurement of a photoluminescence decay of the monolayer MoS_2 at a wavelength of 600 nm [15] and is well correlated with value 33 ps of nonradiative decay for B exciton of the monolayer MoS_2 with 400 nm femtosecond excitation [16]. In contrast to a monolayer, in a few-layer MoS_2, the transition between the valence band and conduction band is indirect [17]. In this case, recombination of an exciton occurs nonradiatively through recombination traps and impurity centers, which are the mediators that transmit the phonon momentum to the lattice and can reduce the relaxation time of photoexcited excitons.

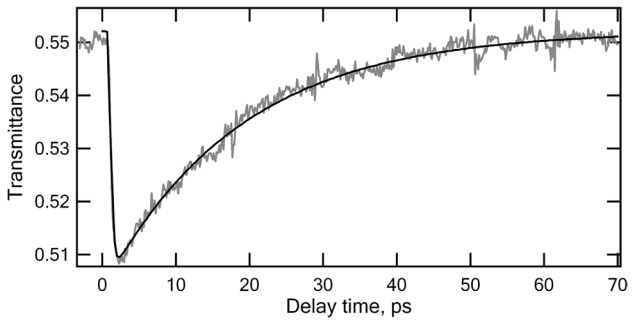

Fig. 6 Time-resolved transmittance of the few-layer MoS_2 on wavelength 514 nm after femtosecond pulsed excitation and the best approximation using Eq. 6

The signal of darkening ($T(t=0) < T(t\to\infty)$) was registered in the pump-to-probe experiment. As it follows from Eq. (6) the signal of darkening occurs if the relation $\sigma_1 > \sigma_0$ is fulfilled. Such relation between intraband and interband absorption cross sections explains experimental data in the following interpretation. The nonlinear absorption of the sample with MoS_2 at low intensities up to 15 GW/cm^2 is due to increasing the carrier population on first conduction band state CB1 and absorption of the transition CB1→CB2. It is sort of reverse saturable absorption (RSA) when the excited-state absorption is large compared to the ground-state absorption which leads to increasing total absorption when going from low to high incident pulse intensity. Saturable absorption at high intensities is due to depletion of the lower band states VB and CB1 and occupation of the second conduction band state CB2 which leads to saturation of the transition CB1→CB2.

In further analysis for low intensities we use the system of only two Eq. 2 and Eq. 3 with approximations $\sigma_1 N_2 << \sigma_0 N_1$ and $N_1 + N_2 \approx N_0$. In addition, the term of TPA is not considered further in our calculations. As it is followed from Eq. 2, we can apply that if the condition $\beta << 2\sigma_0 N_0 / I_0$ is fulfilled. Taking I_0 in the area of nonlinear absorption ~ 10 GW/cm^2 we can estimate the upper value of the two-photon absorption coefficient $\beta << 10^{-9}$ cm/W below which TPA cannot be taken into account. The significant saturation effect appears at high intensities and also confirms the absence of TPA influence and as it follows from Eq. 5 the TPA term should be much less than first term in right side of the equation. The same absence of noticeable two-photon absorption was recorded in solutions of few-layer MoS_2 obtained by chemical and hydrothermal exfoliation of crystalline MoS_2 under excitation by 100 fs pulses at 800 nm [18], at 400 nm [19] and for multilayer MoS_2 under excitation by 10 ps pulses at 532 nm [20]. Taking these approximations, the only first term on the right side of the Eq. 2 remains and further integration over time for a Gaussian-shaped pulse results in the expression:

$$N_1(I_0) = N_0 \exp\left(-\frac{\sigma_0}{\hbar\omega}\int_{-\infty}^{0} I(t)\mathrm{d}t\right) \approx N_0 \exp\left(-\frac{\sigma_0}{\hbar\omega}\frac{I_0 \cdot \tau_p}{2}\right). \quad (7)$$

After substitution of Eq. 7 in Eq. 5 and integration over the sample length without TPA term we can get an expression for nonlinear absorption:

$$\begin{aligned} T(I_0) &= T_0 \exp\left(-\frac{\alpha_0 I_0 \times \tau_p}{2\hbar\omega}(\sigma_1 - \sigma_0)L_{\text{eff}}\right) \\ &= T_0 \exp\left(-\frac{\sigma_0 \alpha_0 I_0 \cdot \tau_p}{2\hbar\omega}(K-1)L_{\text{eff}}\right). \end{aligned} \quad (8)$$

where $K = \sigma_1/\sigma_0$. Rewriting Eq. 8 for Z-scan method:

$$T(I_0, z) = T_0 \exp\left(-\frac{\alpha_0 I_0 \times \tau_p}{2\hbar\omega\left(1 + \left(z/z_0\right)^2\right)}(\sigma_1 - \sigma_0)L_{\text{eff}}\right), \tag{9}$$

where $\alpha_0 = \sigma_0 N_0$, the Rayleigh length $z_0 = \pi r_0^2/\lambda$ and $L_{\text{eff}} = (1 - \exp(-\alpha_0 L))/\alpha_0$.

We used Eq. 9 for fitting experimental curves in Fig. 3 where curve 1 represents the pure nonlinear absorption due to RSA that allowed us to find the value of difference of the absorption cross section $\sigma_1 - \sigma_0 = (1.79 \pm 0.07) \times 10^{-17}$ cm^2. With increasing pulse intensity the peak of SA arises in the center of the nonlinear absorption hollow as it is seen on curve 2 and curve 3. Thus, the curve with saturation peak up has the characteristic wings down when z-coordinate goes to position where intensity is lower. We used part of the wings without central saturation peak to fitting experimental curve 3 on Fig. 3 that yielded the value of σ_1-$\sigma_0 = (1.87 \pm 0.14) \times 10^{-17}$ cm^2 which coincides with the previous value within measurement error. If known value of σ_1-σ_0 and transmittance change $T(t=0) - T(t\to\infty) = 0.04$ from Fig. 6 are substituted into Eq. 6 that allows us to estimate the concentration of the photoinduced carriers on lower-condition band $N_2(0) \sim 3.1 \times 10^{16}$ cm^{-3} after pulsed excitation on intensity 17 GW/cm^2.

To make evolution of the system Eqs. (2–4) at high intensities of incident light where SA was registered we assume approximation $N_2 + N_3 \approx N_0$ and $\tau_p < \tau_1$. Solving the system of Eqs. (3,4) in steady-state condition during pulsed excitation the expression for concentration N_2 is given by

$$N_2(I_0) = N_0 \frac{1}{1 + \frac{I_0}{I_S}}, \tag{10}$$

where

$$I_S = \frac{\hbar\omega}{\sigma_1 \tau_2}. \tag{11}$$

After substituting Eq. 10 in Eq. 5 and integrating over the sample length the transmittance vs intensity can be written as:

$$T(I_0) = \exp\left\{K \frac{I_S}{I_0} \ln\left(1 - \frac{\alpha_0 L}{1 + \frac{I_S}{I_0}}\right)\right\}, \tag{12}$$

with condition $\alpha_0 L I_0 < I_S + I_0$ which is fulfilled for all our experimental cases. Solid line in the Fig. 4 is the best approximation of experimental P-scan curve using Eq. 12 in the SA area (Zone 2) from which the values $K = 1.29 \pm 0.01$ and $I_S = 49 \pm 2$ GW/cm^2 were obtained. Experimental linear transmittance $T_0 = \exp(-\alpha_0 L) = 0.55$ for the length $L = 0.2$ cm gives the linear absorption coefficient $\alpha_0 = 2.95$ cm^{-1}. Best approximation of the P-scan curve in the RSA area (Zone 1) using Eq. 8 and K yields the interband absorption cross section $\sigma_0 = (6.36 \pm 0.46) \times 10^{-17}$ cm^2 by multiplying on K gives the value of intraband absorption cross section $\sigma_1 = (8.2 \pm 0.7) \times 10^{-17}$ cm^2. The measured absorption cross section for interband transition corresponds in order of magnitude to those obtained in [3, 8, 18]. For our knowledge the value of absorption cross section for intraband transition in a 4–5 layer MoS_2 upon green excitation has been obtained for the first time by a direct method. From expression $N_0 = \alpha_0/\sigma_0$ we can determine the value of photoinduced electron–hole density $N_0 = (4.63 \pm 0.34) \times 10^{16}$ cm^{-3}. Using Eq. 11 with known values I_S and σ_1 we can estimate the intraband relaxation time $\tau_2 = 96 \pm 12$ fs. The estimated time of intraband relaxation is three times more than determined in [18] for ultrafast carrier thermalization under excitation at 800 nm to lower-condition band state. For our case the relaxation from high states of condition band CB2 to lower state of condition band CB1 with more energy dissipation can lead to increase of the intraband relaxation time.

3 Conclusion

Nonlinear optical absorption in aqueous suspension of 4–5 layer MoS_2 sheets under femtosecond pulsed excitation at a wavelength of 514 nm were studied. Depending on incident intensity, two regions of nonlinear effects were registered with reverse saturable absorption at low intensity and saturable absorption at high intensity. The 3-level model was proposed for describing experimental data. Using Z- and P-scan methods the intraband and interband absorption cross sections were measured. It was shown that the relation $\sigma_1 > \sigma_0$ between intraband and interband absorption cross sections is needed to explain the nonlinear behavior of the sample with MoS_2. The two-photon absorption was not considered for describing the nonlinear effects. Observed effects can be treated as interplay between rates of one-photon absorptions for interband and intraband transitions.

References

1. D. Jariwala, V.K. Sangwan, L.J. Lauhon, T.J. Marks, M.C. Hersam, ACS Nano **8**, 1102 (2014)
2. M. Zhang, R. Howe, R. Woodward, E.J.R. Kelleher, F. Torrisi, G. Hu, S.V. Popov, J.R. Taylor, T. Hasan, Nano Research **8**, 1522 (2015)
3. Q.Y. Ouyang, H.L. Yu, K. Zhang, Y. Chen, J. Mater. Chem. C **2**, 6319 (2014)
4. H. Xia, H. Li, C. Lan, C. Li, X. Zhang, S. Zhang, Opt. Express **22**, 17341 (2014)

5. R. Wang, B.A. Ruzicka, N. Kumar, M.Z. Bellus, H.-Y. Chiu, H. Zhao, Phys. Rev. B **86**, 045406 (2012)
6. C. Cheng, H. Liu, Z. Shang et al., Optical Mater. Express **6**, 367 (2016)
7. H. Liu, A. Luo, F. Wang et al., Opt. Lett. **39**, 4591 (2014)
8. Y. Li, N. Dong, S. Zhang, X. Zhang, Y. Feng, K. Wang, L. Zhang, J. Wang, Laser Photonics Rev. **9**, 427 (2015)
9. D. Li, W. Xiong, L. Jiang et al., ACS Nano **10**, 3766 (2016)
10. H. Liu, A.-P. Luo, F.-Z. Wang et al., Opt. Lett. **39**, 4591 (2014)
11. D.V. Khudyakov, A.A. Borodkin., A.S. Lobach., A.V. .Ryzhkov, S.K. Vartapetov, Appl. Opt. **52**, 150 (2013)
12. R.A. Bromley, R.B. Murray, A.D. Yoffe, J. Phys. C Solid State Phys. **5**, 759 (1972)
13. H.-P. Komsa, A.V. Krasheninnikov, Phys. Rev. B 86, 241201(R) (2012)
14. A. Kuc, N. Zibouche, T. Heine, Phys. Rev. B **83**, 245213 (2011)
15. T. Korn, S. Heydrich, M. Hirmer, J. Schmutzler, C. Schu¨ller, Appl. Phys. Lett. **99**, 102109 (2011)
16. S.H. Aleithan, M.Y. Livshits, S. Khadka, J.J. Rack, M.E. Kordesch, E. Stinaff, Phys. Rev. B **94**, 035445 (2016)
17. K.F. Mak, C. Lee, J. Hone, J. Shan, T.F. Heinz, Phys. Rev. Lett. **105**, 136805 (2010)
18. K. Wang, J. Wang, J. Fan, M. Lotya et al., ACS Nano **7**, 9260 (2013)
19. H. Zhang, S.B. Lu, J. Zheng, J. Du, S.C. Wen, D.Y. Tang, K.P. Loh, Optics Express **22**, 7249 (2014)
20. J. Zhang, H. Ouyang, X. Zheng et al., Opt. Lett **43**, 243 (2018)